JOURNAL OF MATERIALS SCIENCE 23 (1988) 2533–2545

Ductile-to-brittle transition of rubber-modified polypropylene

Part 2 *Failure mechanics*

C. J. CHOU*, K. VIJAYAN‡, D. KIRBY§, A. HILTNER, E. BAER
Center for Applied Polymer Research and Department of Macromolecular Science, Case Western Reserve University, Cleveland, Ohio 44106, USA

The deformation behaviour of blends of polypropylene (PP) with ethylene–propylene rubber was studied as a function of temperature and composition under tension. The damage ahead of the deliberately introduced defect was traced quantitatively as a function of external load with the aid of intensity analysis. In unmodified PP or in rubber-modified blends, no stable crack growth was obtained up to 99% of the maximum stress. However, a hierarchy of failure events was observed. First, there was a gradual occurrence of a fan-shaped damage zone. Then an intense damage zone initiated. Finally, a slow tearing mode of crack growth occurred at the maximum stress and the sample failed. The size and shape of the damage zone were influenced by temperature, composition and the artificially introduced stress-raiser. Voids were dominant in the fan zone with some crazes close to the intense damage zone. In the intense damage zone, the crazes coalesced to form a network of deformation bands. The description of the fan zone was achieved by a non-linear or elastoplastic failure approach, analogous to the Hilton–Hutchinson formalism, and the analysis of the intense zone by a critical stress instability criterion. There was also a fair correlation with the Dugdale model for the growth of a wedge-like intense damage zone in the specific case of unmodified PP at −40° C.

1. Introduction

In the first part of this work on the ductile–brittle transition of rubber-modified polypropylene, we have analysed the irreversible deformation mechanisms observed after failure [1]. In this part, the failure processes observed during loading will be studied analytically using an applied mechanics approach.

The foundation of classical fracture mechanics evolved by the experimental observation of brittle fracture in metals and glasses [2]. Failure of polymeric systems is different, and many of the theoretical developments in fracture mechanics cannot be applied directly. The classical Dugdale–Barenblatt model [3, 4] assumes a specific yield zone at the crack tip. This simple, yet controversial, model was readily applied to explain the failure of relatively brittle polymers such as polymethyl methacrylate and polystyrene [5–9]. Since the stress state of a brittle polymer during loading can be estimated elegantly using linear elasticity, the concept of linear elastic fracture mechanics (LEFM) was applied to the brittle failure of polymers [10–15]. Without following these more conventional mechanics approaches, crack layer theory has been advanced recently employing the framework of thermodynamics of the irreversible processes to explain the failure of materials. The phenomenological basis for this analysis is the continuous growth of a crack layer (CL) ahead of the crack front followed by discontinuous crack growth. The CL theory has been particularly applied to fatigue failure of polymers such as polypropylene, polystyrene, high-density polyethylene and polycarbonate [16–20].

The theory of plasticity can be applied to explain the instability during failure of ideal ductile materials [21]. This approach was extended through slip-line analysis to define the damage accumulation ahead of the notch-tip [22, 23]. Slip-line analysis was employed to explain shear bands observed during loading of polycarbonate, polyvinyl chloride and polymethyl methacrylate under a flexural mode [24], as well as the nucleation of crazes at impurity sites in polycarbonate at different temperatures [25].

The phenomenological theory of non-linear (or elastoplastic) fracture mechanics was advanced to explain the behaviour of certain ductile metal alloys [26–31]. To date, little attention has been given to the understanding of the failure of polymers using this non-linear approach. The toughness of particulate-filled polymers was explained by developing a non-linear constitutive expression [32]. Realizing that LEFM was not applicable for the study of ductile crystalline polymers such as polyethylene (PE), polypropylene (PP) and PP–PE block copolymers, an approximate nonlinear approach involving the so-called J-energy term was also attempted [33].

In this work, we have studied the deformation

* *Present address*: The Dow Chemical Company, Freeport, Texas 77541, USA.
‡ *Present address*: Richards Medical Company, Memphis, TN 38116, USA.
§ Whirlpool Corporation, Benton Harbor, Michigan 49022, USA.

0022–2461/88 $03.00 + .12

response of both unmodified PP and rubber-modified blends under different conditions. The damage zones which control the failure processes are reported and analysed. The aim of this work is to develop a unified approach which correlates the irreversible deformation processes with the failure mechanics in a ductile polymer system.

2. Experimental procedure

2.1. Sample preparation

The preparation of PP blends with ethylene–propylene rubber (EPR) is described in the previous paper [1]. The injection-moulded plaques had a skin layer 0.1 mm thick that was removed by machining 0.5 mm from both sides of the plaques. Rectangular bars (100 mm × 20 mm × 2.3 mm) were cut from the plaques. Single-edge-notched (SEN) specimens were prepared by slowly pressing a razor blade into the rectangular bar 1 mm deep at the centre of one edge. Notches made at room temperature showed obvious stress-whitening around the cut. To minimize the amount of damage introduced by the notching process, the specimens were first immersed in liquid nitrogen for 1 h before notching. A 1 mm diameter hole was drilled in the centre of other specimens while the specimen was cooled with running ice water. It has been demonstrated that the chosen rectangular sample geometry produces essentially plane stress conditions [12, 13].

2.2. Tensile measurements

The tensile tests were carried out at a crosshead speed of 0.1 mm min^{-1} on an Instron testing machine. A transmission optical microscope system with an attached camera was used to record the damage ahead of the notch tip during loading. The stress applied on the specimens was calculated from the external load and the cross-sectional area of the specimen at the notch tip.

2.3. Damage zone analysis

An Optronics P-1000 rotational drum densitometer, manufactured by Optronics International Inc. (Chelmsford, Massachusetts, USA), was used to analyse the damage zones. The stepping raster and apertures were set at 25 μm, which is the highest resolution available on this instrument. The detector was set at 2D, which gave the best contrast for the negative images analysed. The intensity distribution through the damage zone was obtained by scanning the negative films taken during tensile testing along a series of lines both parallel and perpendicular to the direction of the notch. The trace was extended beyond the damage zone into the region where the light intensity was constant to obtain a baseline.

The deformed specimens were embedded and prepared for optical microscopy by standard metallographic grinding and polishing procedures as described previously [1].

3. Results

3.1. Stress–displacement curves of SEN specimens

The stress–displacement curves of PP at four temperatures from -40 to $+25°$ C are shown in Fig. 1. The curves are displaced 1 mm along the displacement axis. The displacement at fracture increases while fracture stress decreases with increasing temperature. All the curves show non-linear behaviour which becomes more pronounced as the temperature increases. Although it is difficult to define a brittle–ductile transition from the shape of the stress–displacement curves, there is a large increase in non-linear behaviour in the region of T_g, about 0° C.

At $-40°$ C, a small sharp line of damage ahead of the notch tip appeared approximately at Position 1 which is 50% of the maximum stress. The damage grew to a thin wedge shape about 1.5 mm in length before catastrophic fracture. The notch was progressively blunted during loading and no stable crack growth was observed up to 99% of the maximum stress. At 25° C, in contrast to $-40°$ C, a diffuse damage zone ahead of the notch tip appeared at Position 1 which is about 50% of the maximum stress. As the stress increased, the diffuse damage zone expanded into a fan shape and a more intense narrow line of damage formed ahead of the notch tip. Both fan zone and intense damage zone grew as stress increased until catastrophic fracture occurred. Again, the notch was progressively blunted during loading and no stable crack growth was observed up to 99% of the maximum stress. The diffuse damage zone is not seen at $-40°$ C but is first apparent at $-20°$ C. Both diffuse zone and intense damage zone increase in size as the temperature increases. The three positions marked on each curve indicate the stress levels, 0.5, 0.9, and 0.99 of the maximum stress, at which the shape and size of the damage zones will be quantitatively described later.

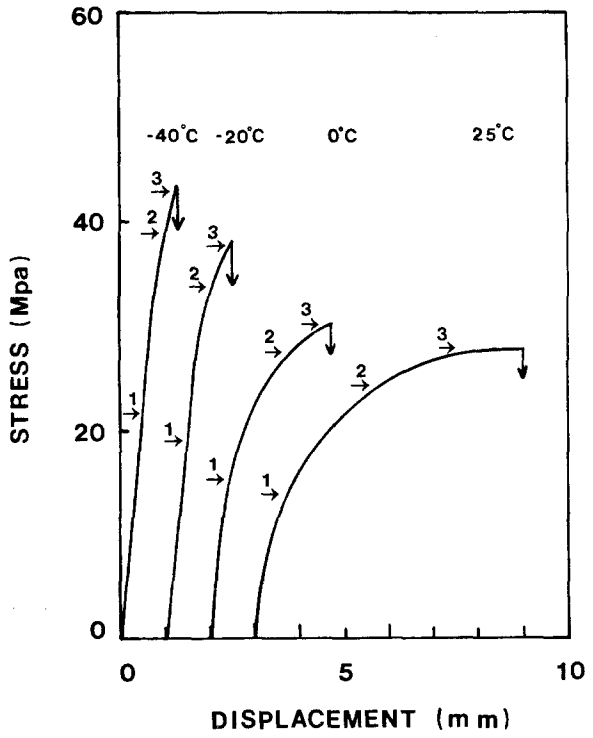

Figure 1 Stress–displacement curves of SEN specimens of unmodified polypropylene at different temperatures.

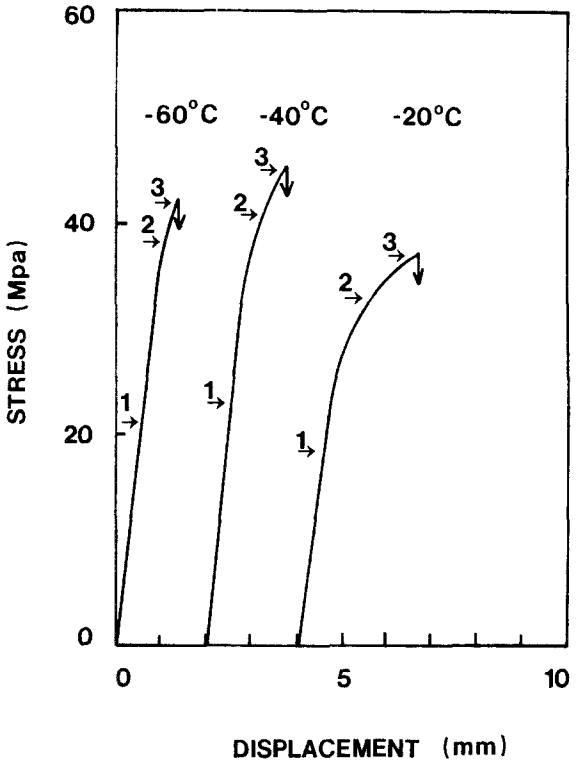

Figure 2 Stress–displacement curves of SEN specimens of 90% PP–10% EPR blend at different temperatures.

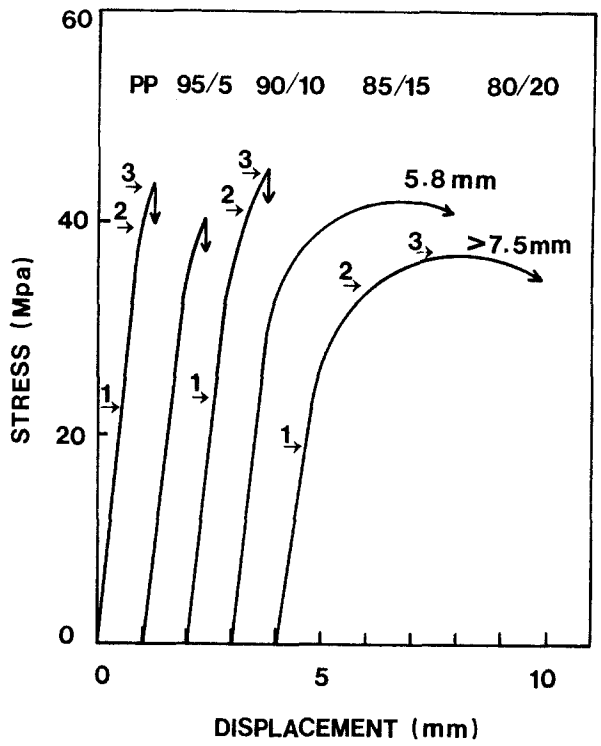

Figure 3 Stress–displacement curves of SEN specimens of PP blends at −40° C.

The stress–displacement curves of 10% EPR blend at three temperatures from −60 to −20° C are shown in Fig. 2. This temperature range encompasses the ductile–brittle (D–B) transition identified in the previous study for this composition [1]. All these curves show a higher degree of non-linear behaviour than those of PP at comparable temperatures. From these curves, the D–B transition seems to occur at about −20° C. Although the transition to less ductile behaviour is conventionally referred to as a brittle-to-ductile transition, it should be emphasized that the non-linearity indicates that some damage accumulation precedes fracture in all cases and truly brittle behaviour is not observed. At all temperatures, a diffuse damage zone was first observed at Position 1 and grew into a fan shape as stress increased. Subsequently, an intense damage zone formed at the notch tip and both fan zone and intense zone expanded until catastrophic fracture occurred. In all cases, the notch was progressively blunted during loading and no stable crack growth was observed up to 99% of the maximum stress. The sizes of the fan zone and intense damage zone increased as temperature increased.

The stress-displacement curves of various compositions at −40° C are shown in Fig. 3. All these curves show non-linear behaviour which becomes more pronounced as rubber content increased. From these stress–displacement curves, it appears that the D–B transition occurred between 10% and 15% EPR. In all blends, both diffuse and intense damage zones initiated and expanded as stress increased. At comparable stresses, the sizes of the two damage zones increases with increasing rubber content. The blends with 10% or less rubber fractured catastrophically at the maximum stress. In 15 and 20% EPR blends, a slow tearing mode of crack growth occurred at the maximum stress. The 15% blend failed at 5.8 mm displacement and the 20% blend did not fail up to 7.5 mm displacement.

3.2. Deformation mechanisms

Longitudinal sections from the core region of the deformed or fractured specimens were examined in the transmission optical microscope to compare the irreversible deformation mechanisms of PP and the blends in the diffuse and intense damage zones. Fig. 4 shows the damage zone ahead of the notch tip in a PP specimen that was fractured at 25° C and polished to about 200 μm thick. A region of intense damage near the fracture site and a surrounding diffuse damage zone that extends some distance away from the fracture site are observed.

Higher magnifications of three locations marked in Fig. 4 are shown in Fig. 5. Fig. 5a shows the highly deformed intense damage zone and dense craze-like damage in the region close to the intense damage zone. Craze-like damage is also seen at b and c in the diffuse damage zone of Fig. 4, as shown in Figs 5b and c. The density and length of the crazes decrease away from the intense damage zone. This confirms the previous observations that at the micro-scale crazing is the primary irreversible deformation mechanism in PP in the ductile-to-brittle transition region [1], and at the macro-scale produces the characteristic stress whitening [17, 34]. By concentrating the stress at a notch, it has been additionally revealed that the craze damage defines two distinct macroscopic damage zones each having its characteristic shape and stress dependence.

Profuse voiding in addition to craze formation was previously observed in the damage zones of PP blends [1]. To confirm these observations, which were made on fractured specimens, a PP blend was loaded to

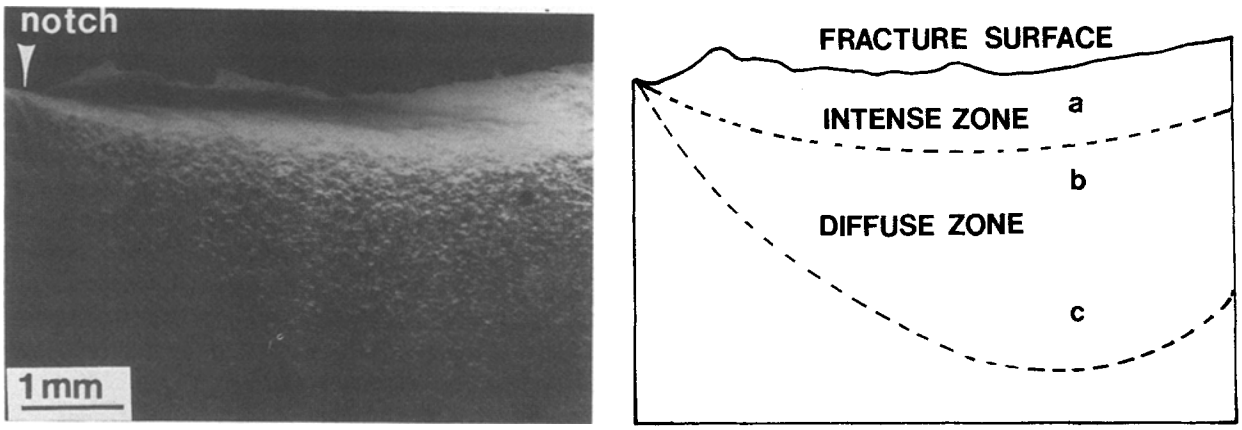

Figure 4 A transmission optical micrograph showing most of the damage zone ahead of the notch tip of unmodified PP fractured at 25° C.

a stress high enough to produce the damage zones but not to fracture the specimen, and subsequently examined in the optical microscope. The specimen was a 10% EPR blend that had been loaded at − 40° C to 90% of the fracture stress and then allowed to relax at − 40° C under fixed elongation for 3 h. Longitudinal sections about 200 μm thick were taken close to the surface and from the core region of the specimen. A micrograph of the damage zone at the core region is shown in Fig. 6. A long narrow intense damage zone surrounded by a large fan-shaped diffuse damage zone is observed. The damage zones observed in the specimen from the surface were very similar to those in Fig. 6 in terms of the size and shape of both intense and diffuse zones, confirming the plane stress state of the thin sample studied.

The core section was further polished to about 40 μm thick and Fig. 7a shows that the intense damage zone consists of a highly deformed region of craze-like damage. In the diffuse zone, some craze-like damage can be observed in the optical microscope close to the intense zone. Damage mechanisms that produce overall stress-whitening of the diffuse zone are not clearly distinguishable at this magnification, although profuse voiding at the rubber particles is described in the previous paper [1] as the cause. Fig. 7b, a higher magnification of a region near the centre of the intense zone, shows crazes in the diffuse damage zone oriented parallel to the intense zone. The length and density of these crazes decrease away from the intense damage zone.

3.3. Growth of damage zones

The existence of both intense and diffuse damage zones and their characteristic appearances at the optical microscope level were described in the previous study that utilized fractured specimens [1]. By deliberately introducing a stress concentration and deforming the specimens at low temperatures, it was possible to observe the growth of the damage zones prior to fracture. The size and shape of the damage zones were analysed by a microdensitometer at three stress levels: 50% of the maximum stress close to damage initi-

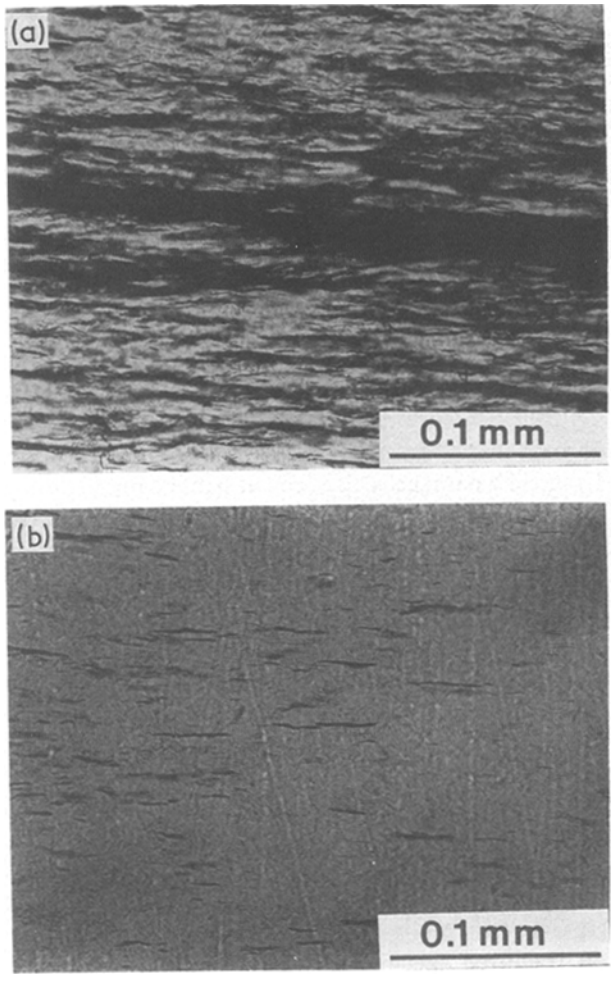

Figure 5 Higher magnification of three regions of the damage zone as indicated in Fig. 4: (a) in the intense damage zone, (b) close to the intense damage zone, (c) in the diffuse damage zone.

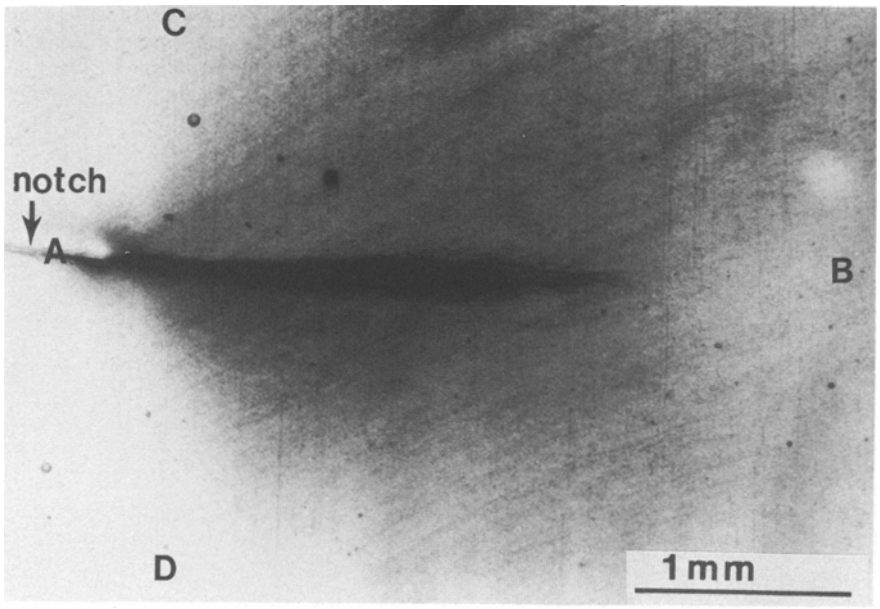

Figure 6 A transmission optical micrograph showing most of the damage zone ahead of the notch tip of 90% PP–10% EPR blend. The specimen was deformed to 90% of the maximum stress at −40° C.

ation, 90% of the maximum stress, and just before failure at 99% of the maximum stress. Even at 99% of the maximum stress, no crack growth was observed in any of the specimens. Fig. 8a shows a typical intensity scan of the photographic negative along the notch direction (marked AB in Fig. 6). The intensity drops sharply at the notch tip and then increases gradually away from the notch tip. The length of the diffuse damage zone (L_d) is determined by the distance from the notch tip to the intersection with the baseline as shown in the figure. Fig. 8b shows the intensity distribution along the load direction (CD in Fig. 6). The width of the diffuse damage zone is determined by the intersections of the base lines. Numerous scans were made in both directions to determine the boundary of the diffuse damage zone. The intense damage zone was directly measured (L_p) from the enlarged image (20×) since the contrast of the intense damage to the diffuse damage is very sharp.

Fig. 9a shows the growth of the damage zones in PP at four temperatures. At 50% of the maximum stress, a small sharp line damage appeared ahead of the notch tip at −40° C that grew into a wedge shape as the stress increased. At −20° C and at higher temperatures, a diffuse damage zone formed before the intense line damage. As the stress increased, the diffuse damage zone at −20° C expanded to a flame shape enclosing the wedge-shaped intense zone. At 0 and 25° C, the diffuse zone assumed a fan shape as it grew. Both damage zones expanded until the specimen fractured. The size of the damage zones increased as temperature increased and notch blunting was much more pronounced at the higher temperatures.

Fig. 10 shows the growth of damage zones in the 10% EPR blend at three temperatures from −60 to −20° C. At all temperatures, a fan-shaped damage zone was observed at Position 1 on the stress–displacement curves or 50% of the maximum stress. The fan zone expanded and a wedge-like intense damage developed at the notch tip as the stress increased. Both damage zones expanded until the specimen fractured. The shape of the two zones did not change but the size increased with increasing temperature and notch blunting became more pronounced. Blend composition has virtually no effect on the shape of the damage zones (Fig. 11) although the increased ductility with higher rubber loading is reflected in a larger fan zone and a wider intense zone with a more blunted notch.

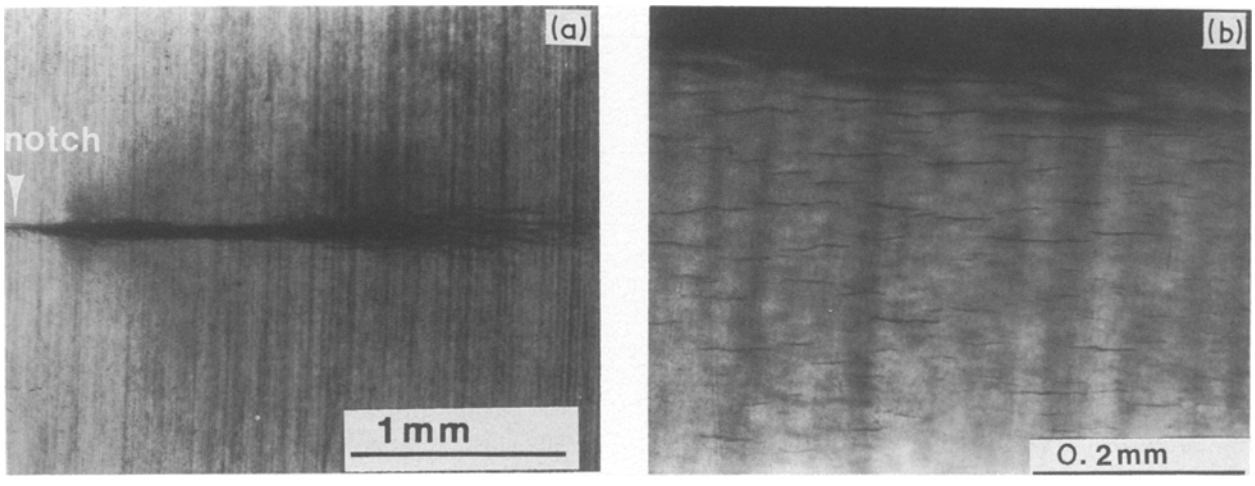

Figure 7 The same specimen as in Fig. 6 after polishing to 20% of the thickness: (a) entire intense zone, (b) a magnified view near the intense damage zone at the centre of (a).

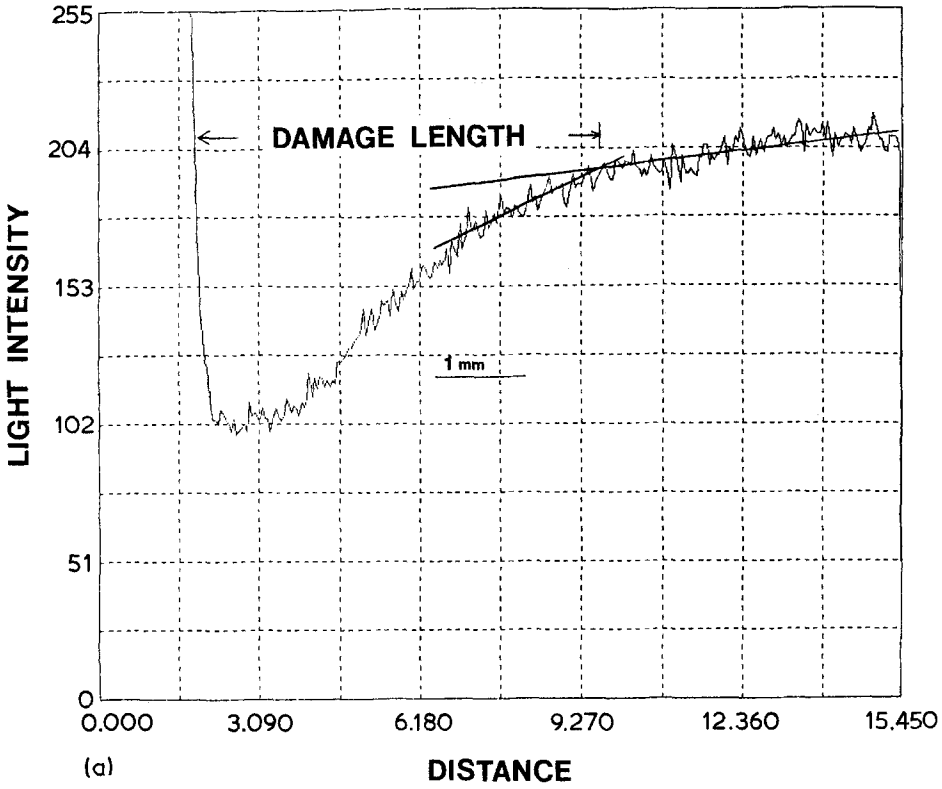

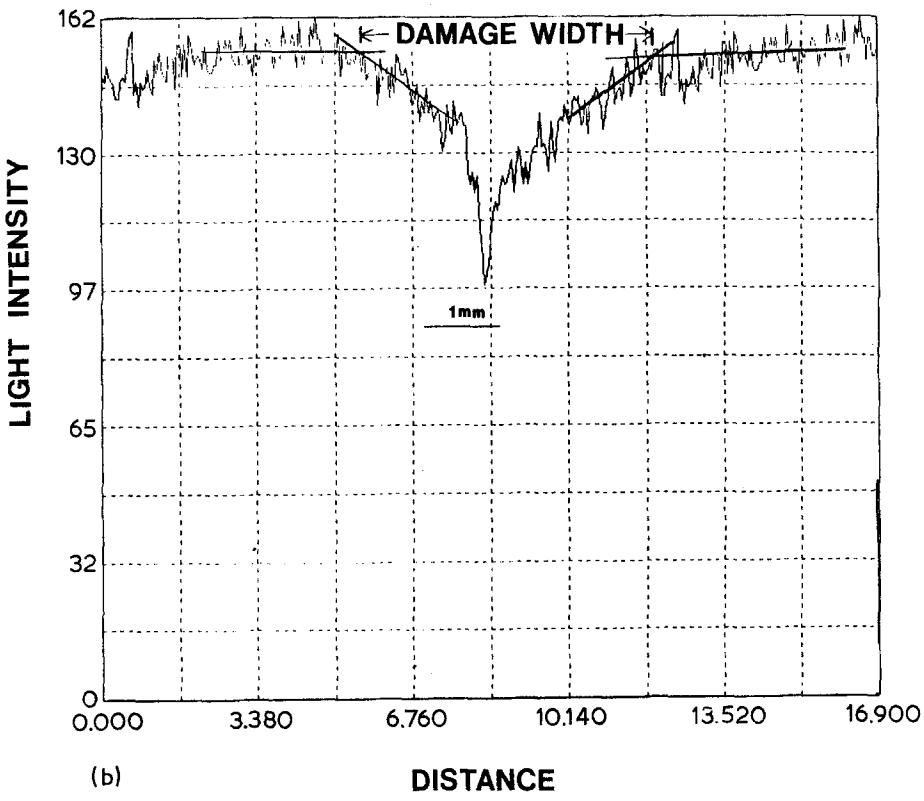

Figure 8 Microdensitometer scans of the damage zone (a) along the notch direction and (b) along the load direction.

In order to make a comparison between PP and the more ductile 10% EPR blend, reference is made to the stress–displacement curves (cf. Figs 2 and 3) where it is noted that the curve for the blend at $-60°$ C is almost identical to that of PP at $-40°$ C. Nevertheless, the damage differs in appearance particularly as regards the diffuse zone which is not observable in PP but clearly present in the blend. Even at higher temperatures where PP does exhibit a diffuse damage zone, the shape is different from that of the blends. Differences in the appearance of the diffuse zone may reflect the different mechanisms by which these materials respond to an imposed external stress. It is recalled that at the microscopic level, crazing was the primary irreversible deformation mechanism throughout the diffuse zone of PP whereas in addition to some craze formation, mostly close to the intense zone, the stress-whitening mechanism that defines the size and shape of the diffuse zone in the blends is profuse voiding at the rubber particles.

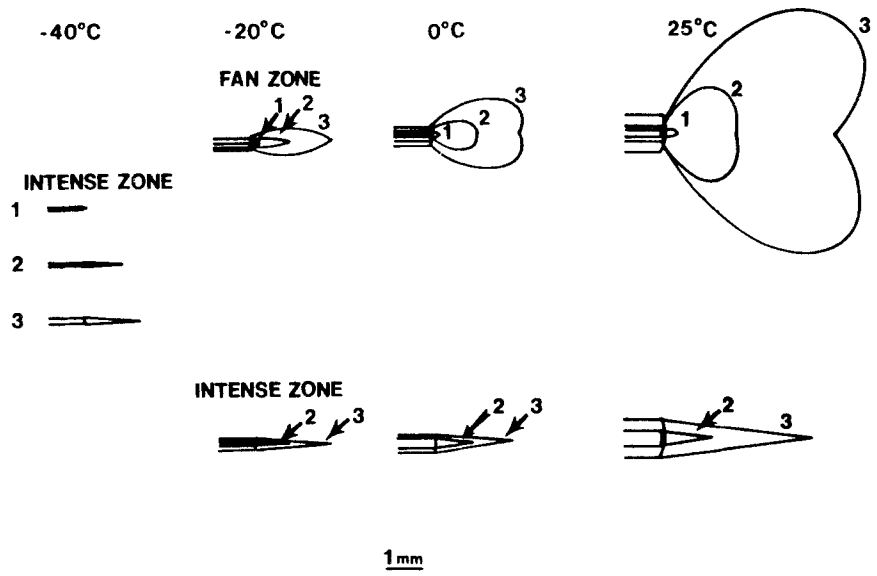

Figure 9 Growth of the damage zones at 0.5, 0.9, and 0.99 of the maximum stress for unmodified PP at different temperatures.

3.4. Deformation at a hole

The stress–displacement curve at $-40°C$ for a 10% EPR specimen with a circular centre hole, shown in Fig. 12, exhibits highly non-linear behaviour at high stresses. Fig. 13 shows a micrograph of the sample after it was deformed to 99% of the maximum stress. A pair of intense damage zones along the equator are seen surrounded by a diffuse fan zone. Faint damage zones occur above and below the hole but only the upper one is barely visible in the photograph.

The four positions marked on the stress–displacement curve indicate the stress levels, 0.76, 0.9, 0.95 and 0.99 of the maximum stress, at which the shape and size of damage zones were analysed (Fig. 14). The pair of fan zones appeared approximately at Position 1 and expanded as stress increased. At 95% of the maximum stress, a pair of intense damage zones formed at the equator of the hole and two faint damage zones appeared above and below the hole, extending outward from the dashed lines in Fig. 14. At 99% of the maximum stress, the fan zone reached the sample edge, and the two faint damage zones spread closer to the hole. During loading, the hole deformed into an ellipse as the intense zone grew into a wedge-shape. No stable crack propagation was observed until the maximum stress was reached and the specimen fractured catastrophically. Compared to the notched geometry, the deformation mechanisms are the same; the only difference is the local stress distribution around the artificial defect which gives rise to a different damage map in the specimen. The higher load required to initiate damage around the hole is simply due to the lower stress intensity factor at a circular hole compared to a sharp notch.

4. Discussion

4.1. Analysis of fan zone

The classical Griffith approach is applicable only for ideal brittle fracture, an extreme case of the linear elastic failure process. Recently there has been considerable progress in the understanding of fracture of relatively brittle polymers from the linear elastic

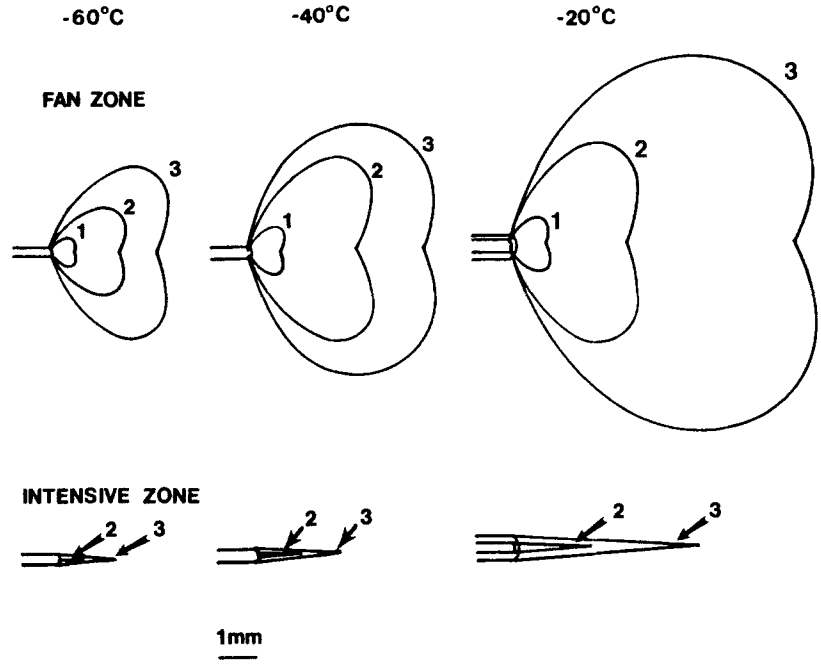

Figure 10 Growth of the damage zones at 0.5, 0.9, and 0.99 of the maximum stress for 90% PP–10% EPR blend at different temperatures.

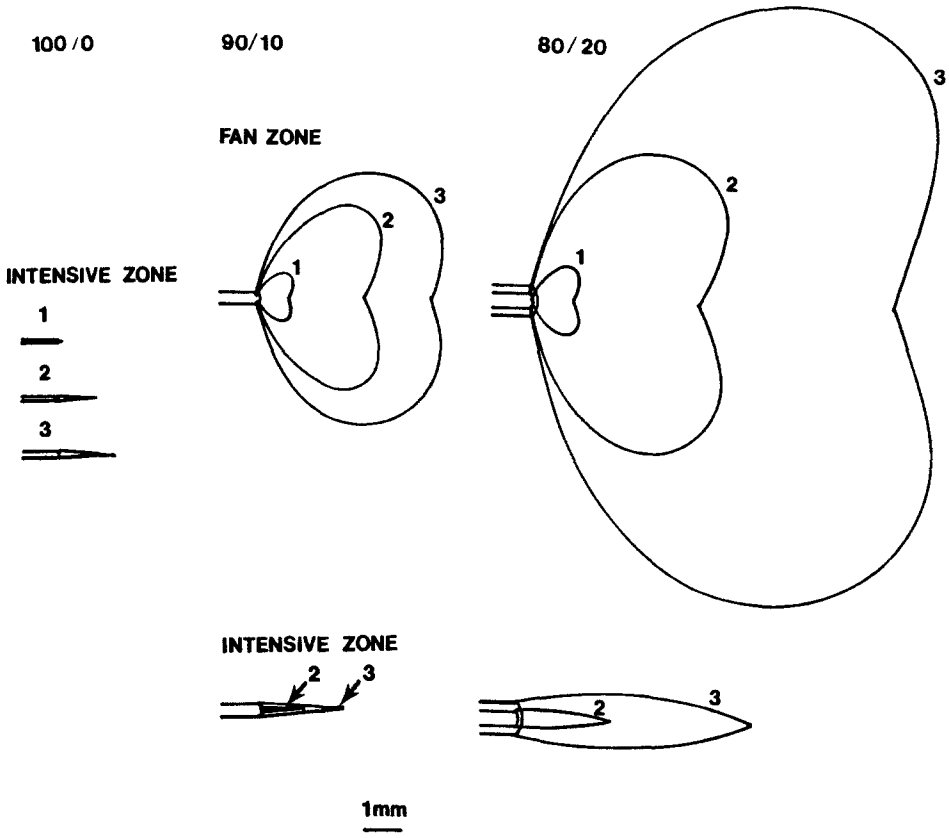

Figure 11 Growth of the damage zones at 0.5, 0.9, and 0.99 of the maximum stress for different compositions at $-40°$ C.

fracture mechanics standpoint [10–14]. The Dugdale model is a specialized phenomenological model that works well for brittle polymers under certain conditions [5–9]. On the other hand, the theory of perfect plasticity may be applied to ideal ductile instability, an extreme case of the non-linear failure process [21]. In our system, we have observed during loading a gradual increase in non-linearity over large strains up to the yield stress. This is an intermediate case between ductile and brittle behaviour. Subsequently, the non-linear or elastoplastic failure approach is envisaged to explain the growth of the fan zone, a precursor to the failure process.

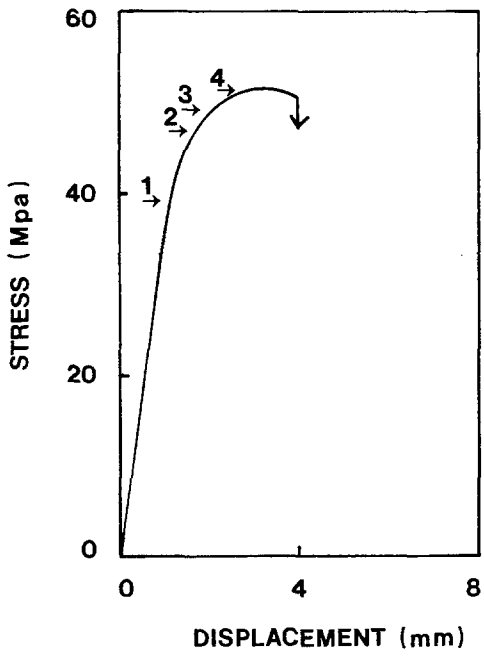

Figure 12 Stress–displacement curves of 90% PP–10% EPR blend with a circular centre hole at $-40°$ C.

In the case of brittle fracture of materials, it is well known that there is some local elastic yielding at the notch tip at higher loading. The size of this small-scale plastic yielding was estimated to be a second-degree function of the external load [35, 36]:

$$\frac{r}{a} = \frac{Y^2}{2\pi}\left(\frac{\sigma}{\sigma_{ys}}\right)^2 f(\theta) \quad (1)$$

where r, θ are Cartesian coordinates, a the notch length, Y a geometrical factor, σ the applied stress, σ_{ys} the yield stress and $f(\theta)$ an angular function. It was also shown that $f(\theta) = \cos^2(\theta/2)[4 - 3\cos^2(\theta/2)]$, under plane stress conditions [37]. From Equation 1, it may be noted that the size of the plastic zone is small and comparable with the notch dimension. The LEFM was successfully applied since the elastic stress state of the entire specimen would be totally dependent upon the notch and the tiny plastic zone. Further, the size of the plastic zone is almost insignificant compared to the sample dimension.

In the case of ductile failure of materials, there is a large-scale non-linear or elastoplastic yielding ahead of the notch tip during loading. Hilton and Hutchinson [38] showed that the size of the elastoplastic zone is a much more complex function of the external load [38]. It was also pointed out that when large-scale yielding occurs, the elastoplastic stress and strain are no longer only dependent on crack length, and may be expressed by functions with higher-order terms of the external load. We adopt a similar elastoplastic approach to explain the development of the fan zone.

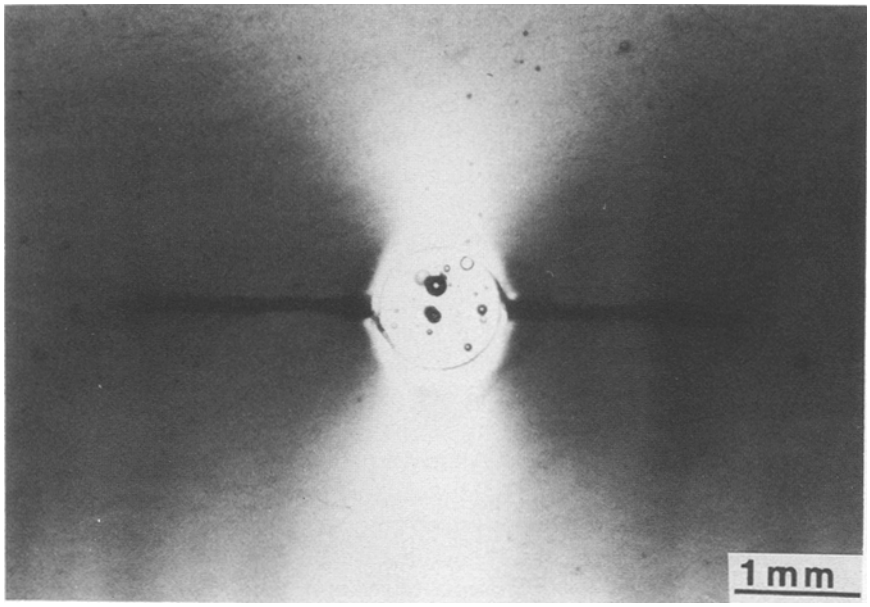

Figure 13 A transmission optical micrograph of the damage zones around the circular hole.

Fig. 15 shows the idealized stress–strain curves in materials with different levels of ductility. The non-linearity in a material is described by gradually increasing values of m. The stress distribution in a highly ductile system is thus assumed to be highly non-linear with strain, as indicated by a higher numerical exponent. At a particular instant of external load σ/σ_{ys}, the ductile notched sample will have a specific stress distribution with the maximum stress at the notch tip. Once the local stress at the notch tip exceeds the elastic limit ($m = 1$), elastoplastic yielding occurs and a tiny diffuse zone nucleates. Then every increment of external load causes expansion of the fan-shaped diffuse zone that defines the elastic–elastoplastic boundary ($m = 1$). Within the fan zone bounded by $m = 1$, m increases to a maximum at the notch-tip.

We start with this general expression:

$$\frac{r}{a} = W\left[A + B\left(\frac{\sigma}{\sigma_{ys}}\right) + C\left(\frac{\sigma}{\sigma_{ys}}\right)^2 + \ldots\right]^{m+1} g(\theta) \quad (2)$$

By using appropriate coefficients and angular functions, the data in Figs 9 to 11 can be adequately described by neglecting all but one term in Equation 2:

$$\frac{r}{a} = W\left[B\left(\frac{\sigma}{\sigma_{ys}}\right)\right]^{m+1} g(\theta) \quad (3)$$

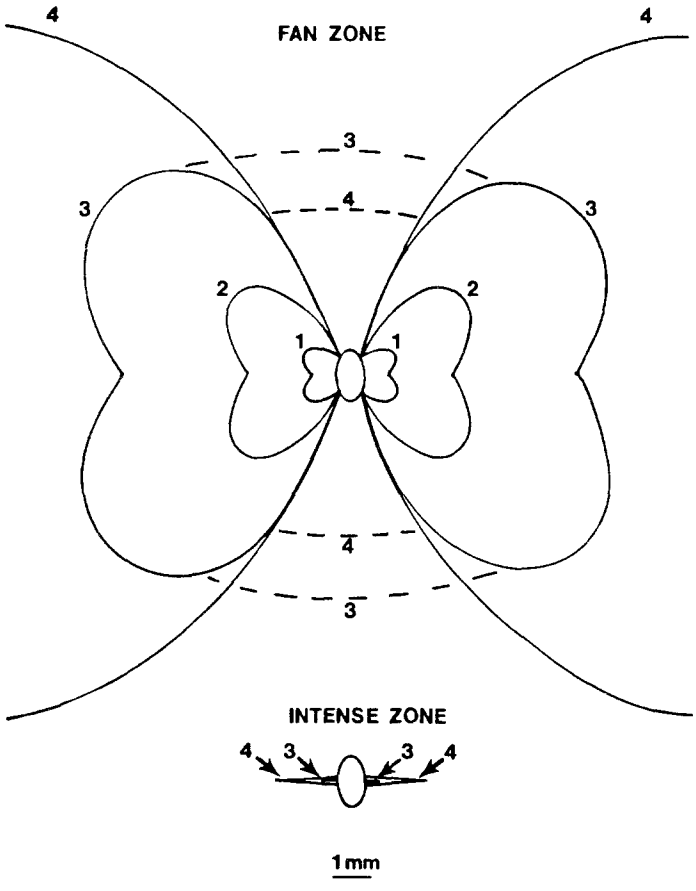

Figure 14 Growth of the damage zones around a 1 mm circular hole at (1) 0.76, (2) 0.90, (3) 0.95, and (4) 0.99 of the maximum stress. 90% PP–10% EPR, −40° C.

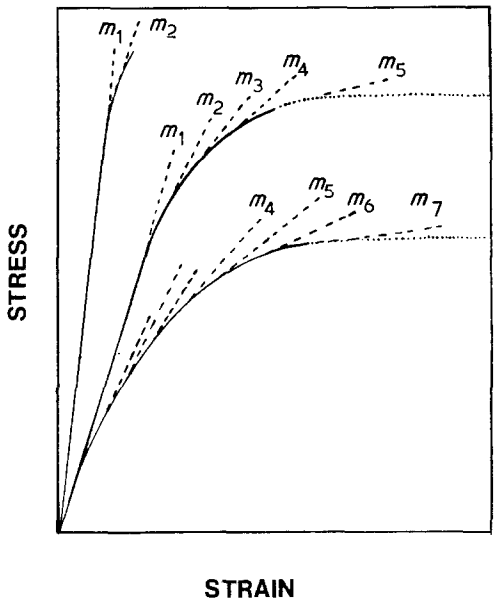

Figure 15 Idealized stress–strain curves of brittle and ductile polymeric materials. For linear elasticity $m = 1$; for ideal plasticity $m = \infty$.

In this equation, W is a constant combining material parameters and geometry factors, B is a fractional number and $g(\theta)$ is a function that describes the shape of the fan zone. If we assume that the fan zone is the boundary of linear elastic behaviour where $m = 1$, the above equation reduces to a form similar to Equation 1. Then the length L_d of the fan zone in the x direction where $g(\theta) = 1$ is given by

$$\frac{L_d}{a} = W\left[B\left(\frac{\sigma}{\sigma_{ys}}\right)\right]^2 \quad (4)$$

The measured length of the fan zone along the x axis is plotted according to Equation 4 for various compositions of rubber-modified polypropylene at $-40°$ C and for the 10% EPR blend at various temperatures in Fig. 16. The values of σ_{ys} were taken from the unnotched stress–strain curves in the previous publication [1]. Comparison of the data with the line of slope equal to 2 shows that the boundary of the fan zone can be represented by the onset of non-linear behaviour. When each set of data is analysed separately by non-linear square fitting, values of m ranging from 0.97 to 1.56 with regression coefficients greater than 0.96 are obtained.

Equation 3 was used to compare the experimental data for the 10% EPR blend at $-40°$ C (Fig. 10). The best fit, as shown in Fig. 17, was obtained using the constants $A = 7.26$, $B = 0.85$ to represent the size and the function $g(\theta) = \cos^{1/2}(5\theta/4)[1 + \sin^2(5\theta/4)]$ to represent the shape of the fan zone.

The experimental fan zone data of unmodified PP at 25° C gave an m value of 2.31 when plotted according to Equation 4. Consequently, we believe that the true fan zone in polypropylene cannot be seen with our optical method. In the case of rubber-modified PP, the previously described voiding mechanism [1] produces intense light scattering which reveals the entire fan zone. Conversely, the irreversible processes that mark the onset of non-linearity in unmodified PP are possibly shear processes that are not seen by our technique.

4.2. Analysis of intense damage zone

The failure analysis of our system must extend over the entire region from ductile to brittle behaviour. Since we have previously shown that unmodified PP and its rubber-modified blends exhibit gradual non-linear behaviour leading towards a yield stress, ideal plastic analysis would obviously not serve our purpose. Subsequently, we proceeded to use the non-linear elastic analysis of Hilton and Hutchinson [38] to describe the non-linear stress–strain behaviour that produces the large diffuse fan zone for our system. Our observations also indicated the development of an intense damage zone which varies in shape with composition and temperature. Assuming that the intense zone initiates when the elastoplastic stress state reaches a critical level, we may describe the intense zone as a "critical fan zone".

The measured length of the intense zone along the x axis is plotted in the same manner as Equation 4 for various compositions of blends and various temperatures in Fig. 18. Each set of data fits a straight line, and analysis by non-linear square fitting shows that the critical m value of the 10% EPR blend increases from 1.76 to 6.95 by increasing the temperature from -60

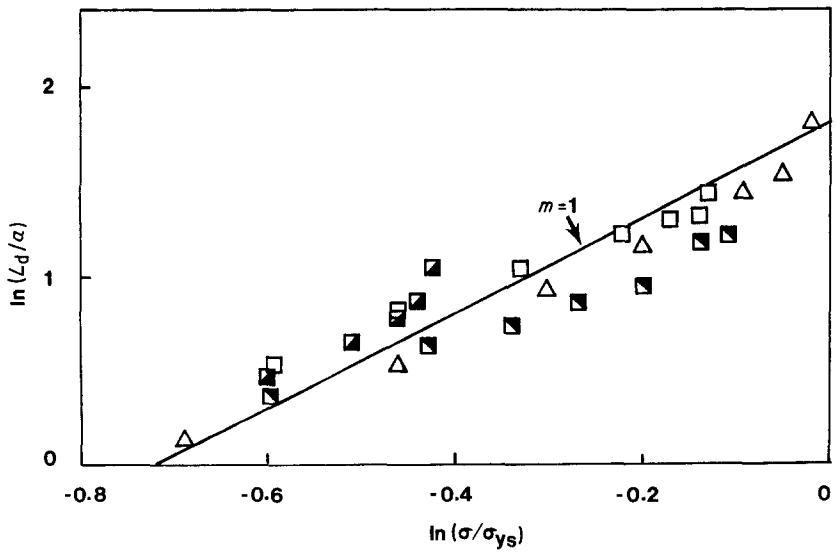

Figure 16 Logarithmic plot of the experimental data for the fan zone with the external load. For 90% PP–10% EPR: (◪) $-60°$ C, $m = 1.06$; (□) $-40°$ C, $m = 0.97$; (◹) $-20°$ C, $m = 1.56$. For 80% PP–20% PP: (△) $-40°$ C, $m = 1.16$.

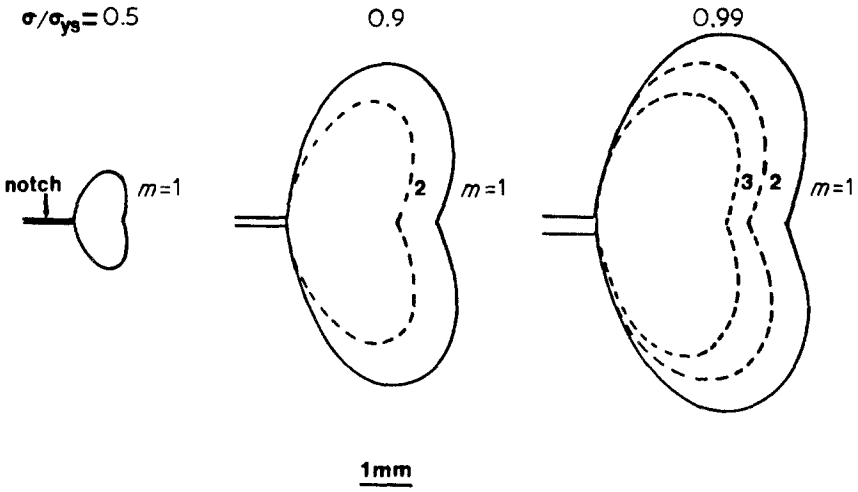

Figure 17 Simulated growth of the fan zone of 90% PP–10% EPR blend at −40° C showing different levels of elastoplastic yielding.

to −20° C. Furthermore, at −40° C the critical m value of the 20% EPR blend (5.00) is larger than that of the 10% blend (3.05). It must be noted that the elastoplastic approach does not predict any singular value of m, only that it will be infinity at the notch tip. The boundary between elastoplastic (fan zone) and plastic (intense zone) behaviour is obtained from the experimental data and permits a critical m value to be calculated. This artificial interface depends on the nature of non-linearity for a specific material (cf. Fig. 15). A larger critical m value represents a larger amount of elastoplastic yielding and a larger fan zone.

The intense zone may also be simply analysed using a critical stress criterion. The controlling stress is along the line of fracture and was estimated from linear elastic analysis of the stress distribution. We treat the problem of loading of an SEN sample by considering the elastic stress component σ_z around a semi-elliptical hole [39]:

$$\sigma_z = \frac{\sigma}{2}\left[2 + \left(\frac{a}{x}\right)^2 + 3\left(\frac{a}{x}\right)^4\right] \quad (5)$$

We have not considered the other normal stress component σ_x and the shear stress component τ_{zx} which are smaller than σ_z. In this approach, the value of x where σ_z reaches a critical value, assumed to be the yield stress σ_{ys}, is related to the length of the intense zone, $x = L_{p+a}$. With reference to the external load σ, Equation 5 gives

$$\frac{L_p}{a} = \left\{\frac{1 + [1 + 24\,((\sigma_{ys}/\sigma) - 1)]^{1/2}}{4[(\sigma_{ys}/\sigma) - 1]}\right\}^{1/2} - 1 \quad (6)$$

This prediction is compared with the experimental data for three compositions in Fig. 19.

An alternative approach, the Dugdale–Barenblatt model [3, 4], assumes a strip of yielded zone emanating from the crack tip described by

$$\left(\frac{L_p}{a}\right) = \sec\left(\frac{\pi\sigma}{2\sigma_{ys}}\right) - 1 \quad (7)$$

This prediction is also plotted in Fig. 19. The intense damage zone does not have the geometry required by Dugdale in many instances. Only in the case of unmodified PP at −40.0° C was there a fair correlation observed with this specialized failure model. In all other instances, the intense zone fits the maximum stress instability condition. Subsequently, a comprehensive description of the ductile-to-brittle transition was achieved by considering the actual stress–strain properties of the material including the progression of elastic, elastoplastic and yield characteristics.

5. Conclusions

1. The failure processes in notched specimens of a PP–EPR blend system were studied under tension.

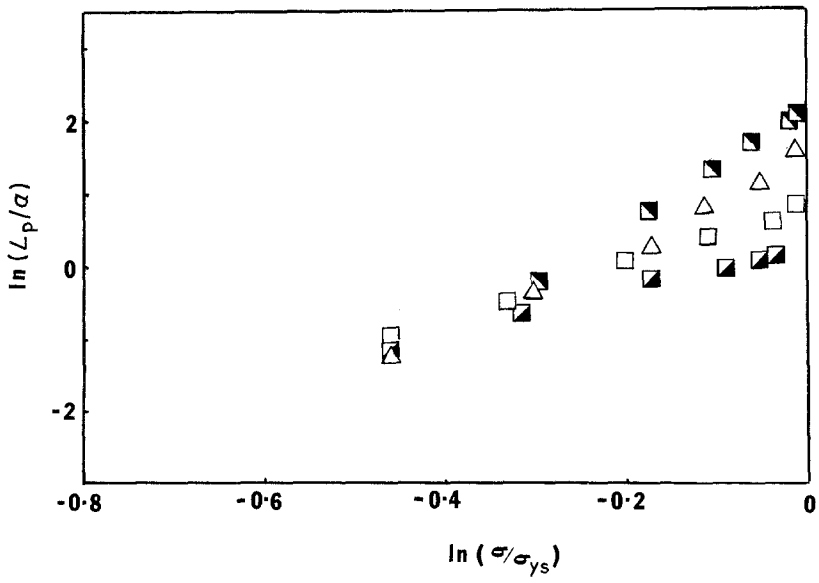

Figure 18 Logarithmic plot of the experimental data for the intense zone with the external load. For 90% PP–10% EPR: (◪) −60° C, m = 1.76; (□) −40° C, m = 3.05; (◥) −20° C, m = 6.95. For 80% PP–20% EPR: (△) −40° C, m = 5.00.

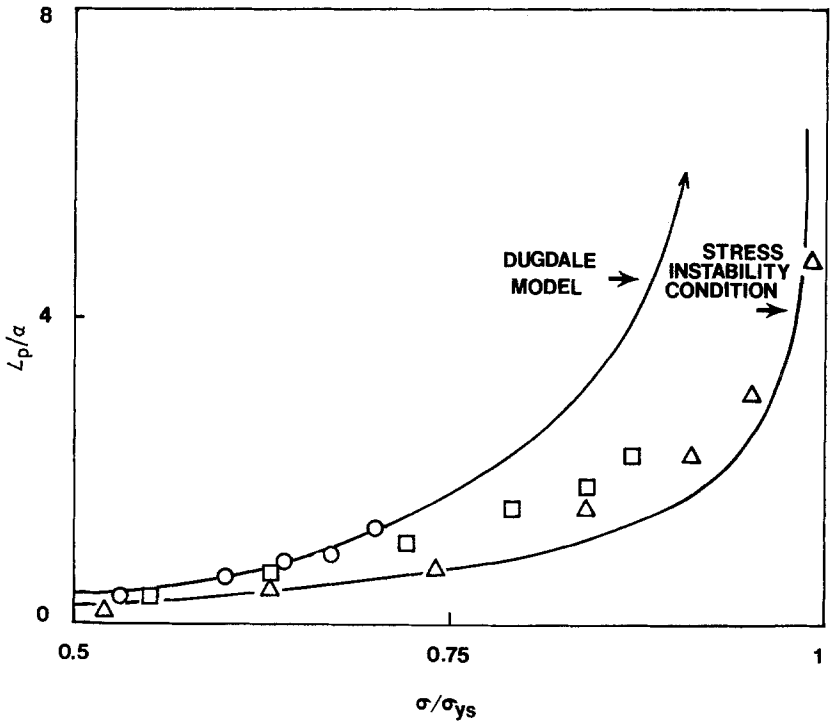

Figure 19 Comparison of maximum stress instability and Dugdale predictions with the experimental data for the intense zone at $-40°$ C: (○) PP, (□) 90% PP–10% EPR, (△) 80% PP–20% EPR.

During loading, a fan-shaped diffuse damage zone formed first ahead of the notch tip, followed by an intense damage zone. These damage zones expanded until the specimen failed. The size and shape of the damage zones were influenced by temperature, composition, and geometry of the stress-raiser.

2. Different mechanisms are active in the growth of these damage zones. In the case of rubber-modified blends, microvoids are dominant in the fan zone with some crazes close to the intense zone. In the case of unmodified polypropylene, only crazes were observed. In both cases, the crazes coalesced to form a network of deformation bands in the intense zone.

3. The development of the damage zones was treated analytically. The Hilton–Hutchinson formalism of elastoplastic failure was successfully applied to the growth of the fan zone. A critical stress instability criterion was found to describe the growth of the intense zone, whereas the Dugdale model was useful only in the specific case of unmodified PP at $-40°$ C.

Acknowledgements

The authors gratefully acknowledge the financial support of the Whirlpool Corporation and the Army Research Office (DAA629-84-K-0155). This work was carried out in the Center for Applied Polymer Research at Case Western Reserve University.

References

1. C. J. CHOU, K. VIJAYAN, D. KIRBY, A. HILTNER and E. BAER, *J. Mater. Sci.* **23** (1988) 000.
2. A. A. GRIFFITH, *Trans. R. Soc.* **221** (1920) 163 (republished with additional comments in *Trans. ASM* **61** (1968) 871).
3. D. S. DUGDALE, *J. Mech. Phys. Solids* **8** (1960) 100.
4. D. I. BARENBLATT, *Adv. Appl. Mech.* **7** (1962) 55.
5. S. K. BHATTACHARYA and N. BROWN, *J. Mater. Sci.* **20** (1985) 2767.
6. W. DOELL, L. KOENCZOE and M. G. SCHINKER, *Polymer* **24** (1983) 1213.
7. H. R. BROWN and I. M. WARD, *ibid.* **14** (1973) 469.
8. J. P. ELINK, J. C. BAUMENS and G. HOWES, *Int. J. Fract. Mech.* **7** (1971) 277.
9. M. SKIBO, R. W. HERTZBERG and J. A. MANSON, *J. Mater. Sci.* **11** (1976) 479.
10. S. HASHEMI and J. G. WILLIAMS, *ibid.* **19** (1984) 3746.
11. *Idem, Polym. Eng. Sci.* **26** (1986) 760.
12. P. L. FERNANDO and J. G. WILLIAMS, *ibid.* **20** (1980) 215.
13. *Idem, ibid.* **21** (1981) 1003.
14. A. CARPINTERI, C. MAREGA and A. SAVADORI, *J. Mater. Sci.* **21** (1986) 4173.
15. F. COPPOLA, R. GRECO and G. RAGOSTA, *ibid.* **21** (1986) 1775.
16. A. CHUDNOVSKY, "The Crack Layer Theory", NASA Report (Case Western Reserve University, Cleveland, Ohio 1983).
17. A. CHUDNOVSKY, A. MOET, R. J. BANKERT and M. T. TAKEMORI, *J. Appl. Phys.* **54** (1983) 10.
18. J. BOTSIS, A. CHUDNOVSKY and A. MOET, *Int. J. Fract.* **33** (1987) 263.
19. K. SEHANOBISH, A. MOET and A. CHUDNOVSKY, *Polymer* **28** (1987) 1315.
20. N. HADDAOUI, A. CHUDNOVSKY and A. MOET, *ibid.* **27** (1986) 1377.
21. R. HILL, in "The Mathematical Theory of Plasticity" (Oxford University Press, London, 1950).
22. R. M. McMEEKING, *J. Mech. Phys. Solids* **25** (1977) 357.
23. *Idem, J. Eng. Mat. Technol.* **99** (1977) 290.
24. M. KITAGAWA, *J. Mater. Sci.* **17** (1982) 2514.
25. R. P. KAMBOUR, M. A. VALLANCE, E. A. FARRAYE and L. A. GRIMALDI, *ibid.* **21** (1986) 2435.
26. G. T. HAHN and A. R. ROSENFIELD, *Acta Metall.* **13** (1965) 293.
27. J. W. HUTCHINSON, *J. Mech. Phys. Solids* **16** (1968) 13.
28. J. R. RICE, *J. Appl. Mech.* **35** (1968) 379.
29. R. M. McMEEKING and D. M. PARKS, ASTM STP 668 (American Society for Testing of Materials, Philadelphia, 1979) p. 379.
30. J. W. HUTCHINSON, "A Course on Nonlinear Fracture Mechanics" (Technical University of Denmark, 1979).
31. *Idem, Trans. ASME* **50** (1983) 1042.
32. A. G. EVANS, S. WILLIAMS and P. W. R. BEAUMONT, *J. Mater. Sci.* **20** (1985) 3668.
33. I. NARISAWA, *Polym. Eng. Sci.* **27** (1987) 41.
34. B. J. JANG, D. R. UHLMANN and J. B. VANDER SANDE, *ibid.* **25** (1985) 98.
35. G. R. IRWIN, in "Handbuch der Physik", Vol. VI

(Springer, Berlin, 1958) p. 551.
36. F. A. McCLINTOCK and G. R. IRWIN, ASTM STP 381 (American Society for Testing and Materials, 1965) p. 84.
37. J. G. WILLIAMS, in "Fracture Mechanics of Polymers" (Ellis Horwood, Chichester, England, 1984) p. 98.
38. P. D. HILTON and J. W. HUTCHINSON, *Eng. Fract. Mech.* **3** (1971) 435.
39. J. G. WILLIAMS, in "Stress Analysis of Polymers" (Wiley, New York, 1973) p. 225.

Received 20 July
and accepted 9 October 1987